Vol. 688: 19–31, 2022
https://doi.org/10.3354/meps14021

MARINE ECOLOGY PROGRESS SERIES
Mar Ecol Prog Ser

Published April 28

Benthic O_2 uptake by coral gardens at the Condor seamount (Azores)

Lorenzo Rovelli[1,8,*], Marina Carreiro-Silva[2,3], Karl M. Attard[1,4,5], Maria Rakka[2,3], Carlos Dominguez-Carrió[2,3], Meri Bilan[2,3], Sabena Blackbird[6], Telmo Morato[2,3], George A. Wolff[6], Ronnie N. Glud[1,5,7]

[1]HADAL & Nordcee, Department of Biology, University of Southern Denmark, 5230 Odense M, Denmark
[2]IMAR – Instituto do Mar, Universidade dos Açores, 9901-862 Horta, Portugal
[3]Instituto de Investigação em Ciências do Mar – Okeanos, Universidade dos Açores, 9901-862 Horta, Portugal
[4]Tvärminne Zoological Station, University of Helsinki, 10900 Hanko, Finland
[5]Danish Institute of Advanced Study – DIAS, University of Southern Denmark, 5230 Odense M, Denmark
[6]School of Environmental Sciences, University of Liverpool, L69 3GP Liverpool, UK
[7]Department of Ocean and Environmental Sciences, Tokyo University of Marine Science and Technology, 108-8477 Tokyo, Japan
[8]*Present address:* iES – Institute for Environmental Sciences, University of Koblenz-Landau, 76829 Landau, Germany

ABSTRACT: Using the non-invasive aquatic eddy covariance technique, we provide the first oxygen (O_2) uptake rates from within coral gardens at the Condor seamount (Azores). To explore some of the key drivers of the benthic O_2 demand, we obtained benthic images, quantified local hydrodynamics, and estimated phototrophic biomass and deposition dynamics with a long-term moored sediment trap. The coral gardens were dominated by the octocorals *Viminella flagellum* and *Dentomuricea* aff. *meteor*. Daily rates of O_2 uptake within 3 targeted coral garden sites (203 to 206 m depth) ranged from 10.0 ± 0.88 to 18.8 ± 2.0 mmol m^{-2} d^{-1} (mean ± SE) and were up to 10 times higher than 2 local sandy reference sites within the seamount summit area. The overall mean O_2 uptake rate for the garden (13.4 mmol m^{-2} d^{-1}) was twice the global mean for sedimentary habitats at comparable depths. Combined with parallel *ex situ* incubations, the results suggest that the octocorals might contribute just ~5% of the observed O_2 uptake rates. Deposition of particulate organic matter (POM) assessed by the sediment trap accounted for less than 10% of the O_2 demand of the coral garden, implying a substantial POM supply circumventing the deployed traps. Our results expand the database for carbon turnover rates in cold-water coral habitats by including the first estimates from these largely understudied coral gardens.

KEY WORDS: Aquatic eddy covariance · Cold-water corals · Condor seamount · Community oxygen uptake · *Viminella flagellum* · *Dentomuricea* aff. *meteor*

1. INTRODUCTION

Cold-water corals (CWCs) are important ecosystem engineers at continental shelves, slopes, seamounts and ridge systems (Roberts et al. 2006, 2009). Habitats formed by CWCs include reefs produced by Scleractinia species (stony corals) and coral gardens formed by Alcyonacea (gorgonians and soft corals), Antipatharia (black corals) and Stylasteridae (lace corals) (Buhl-Mortensen & Buhl-Mortensen 2018). These communities enhance biodiversity and biomass at the deep seafloor by providing complex 3-dimensional structures used as shelter, breeding and feeding grounds for other organisms (Buhl-

*Corresponding author: lorenzo@biology.sdu.dk

Publisher: Inter-Research · www.int-res.com

Mortensen et al. 2010, 2017, Henry & Roberts 2017). The extent and complexity of CWC reefs formed by stony corals have been intensively studied (Davies & Guinotte 2011) and their role as hotspots of carbon and nitrogen cycling in the North Atlantic has been documented by a number of studies (van Oevelen et al. 2009, White et al. 2012, Cathalot et al. 2015, Rovelli et al. 2015, de Froe et al. 2019, De Clippele et al. 2021). In contrast, and despite their widespread occurrence, the importance of CWC gardens remains largely unexplored (Yesson et al. 2012, Rossi et al. 2017, Buhl-Mortensen & Buhl-Mortensen 2018).

Traditionally, the importance of CWC habitats for benthic carbon cycling has been assessed by *ex situ* and *in situ* incubations of coral fragments (Dodds et al. 2007, Khripounoff et al. 2014) or subsamples taken from the CWC community (de Froe et al. 2019). However, this invasive approach can change important hydrodynamic drivers and thus only poorly represents the complex 3-dimensional structures that make up these natural communities. To overcome such shortcomings, non-invasive approaches, most notably open water-based dissolved oxygen (O_2) budget methods (see White et al. 2012) and the aquatic eddy covariance (AEC) technique (Cathalot et al. 2015, Rovelli et al. 2015, de Froe et al. 2019) have been applied. Open-water approaches are limited to settings with a constrained hydrodynamic regime, e.g. canyon-like settings with a dominant flow direction and quantifiable water residence time, and are thus not ideal for natural CWC habitats, which are often characterized by complex hydrodynamics. In contrast, the AEC technique is more widely applicable to CWC reefs, tropical reefs and other complex benthic ecosystems where it has provided spatially and temporally integrated assessments of the O_2 exchange (Long et al. 2013, Cathalot et al. 2015, Rovelli et al. 2015, 2019), and ultimately contributed to advance our understanding of the local carbon turnover for those habitats.

In this study, we applied AEC to quantify and characterize the O_2 uptake rates of a coral garden formed by the octocorals *Viminella flagellum* and *Dentomuricea* aff. *meteor* on the summit of the Condor seamount (Azores). The island slope and seamount habitats of the Azores are mostly dominated by coral gardens (Tempera et al. 2012, 2013), which are key communities for regional biodiversity and potentially for carbon and nutrient cycling (Porteiro et al. 2013, Carreiro-Silva et al. 2017, Gomes-Pereira et al. 2017, Rakka et al. 2021). Measurements of community respiration rates were complemented with (1) octocoral density data obtained from underwater images, (2) water column profiling (e.g. temperature, turbidity, chlorophyll *a*), (3) discrete water samples to characterize nutrient availability and suspended particulate organic matter (POM) and (4) data from a sediment trap mooring to investigate POM supply to the seamount. This study aims to provide insights into the importance of octocoral gardens for benthic carbon cycling in this important oceanic region.

2. MATERIALS AND METHODS

2.1. Study site

The Condor seamount is a linear volcanic ridge situated 17 km south-west of Faial Island, in the Azores archipelago, in the north-east Atlantic (Fig. 1). The seamount measures 39 km in length and rises from 2000 m to a flattened summit at 184 m water depth (Tempera et al. 2013). The summit area (<300 m depth) encompasses an approximate surface of 6.85 km^2 (Pham et al. 2013). Benthic habitats consist of unconsolidated sandy sediments transitioning to hard substrates, covering up to 80% of the summit area. Hard-substrate habitats are characterized by the presence of coral gardens, mostly dominated by the octocorals *Viminella flagellum* and *Dentomuricea* aff. *meteor* (Tempera et al. 2012, Porteiro et al. 2013). Although monospecific coral gardens of *V. flagellum* and *D.* aff. *meteor* are also present within the summit area, the most prominent gardens encompass both coral species, often in conjunction with tall hydrozoans, e.g. *Polyplumaria flabellata* and *Lytocarpia myriophyllum* (Tempera et al. 2012). The seamount induces an anticyclonic Taylor cap over the summit, i.e. an enclosed circulation with mean near-bottom flow velocities of approximately 4 cm s^{-1} (Bashmachnikov et al. 2013), which might promote the retention of organic matter and enhance local productivity (see White et al. 2008). The water column above the seamount is characterized by strong seasonal dynamics in salinity, dissolved O_2 and chlorophyll *a* (chl *a*) concentrations, which is also reflected in the zooplankton and phytoplankton abundance and distribution (Carmo et al. 2013, Santos et al. 2013).

2.2. Selection of sites for AEC deployments, coral densities and sizes

Video images used to select suitable areas for AEC deployments were recorded by means of the towed camera system from the R/V 'Pelagia' (Royal Nether-

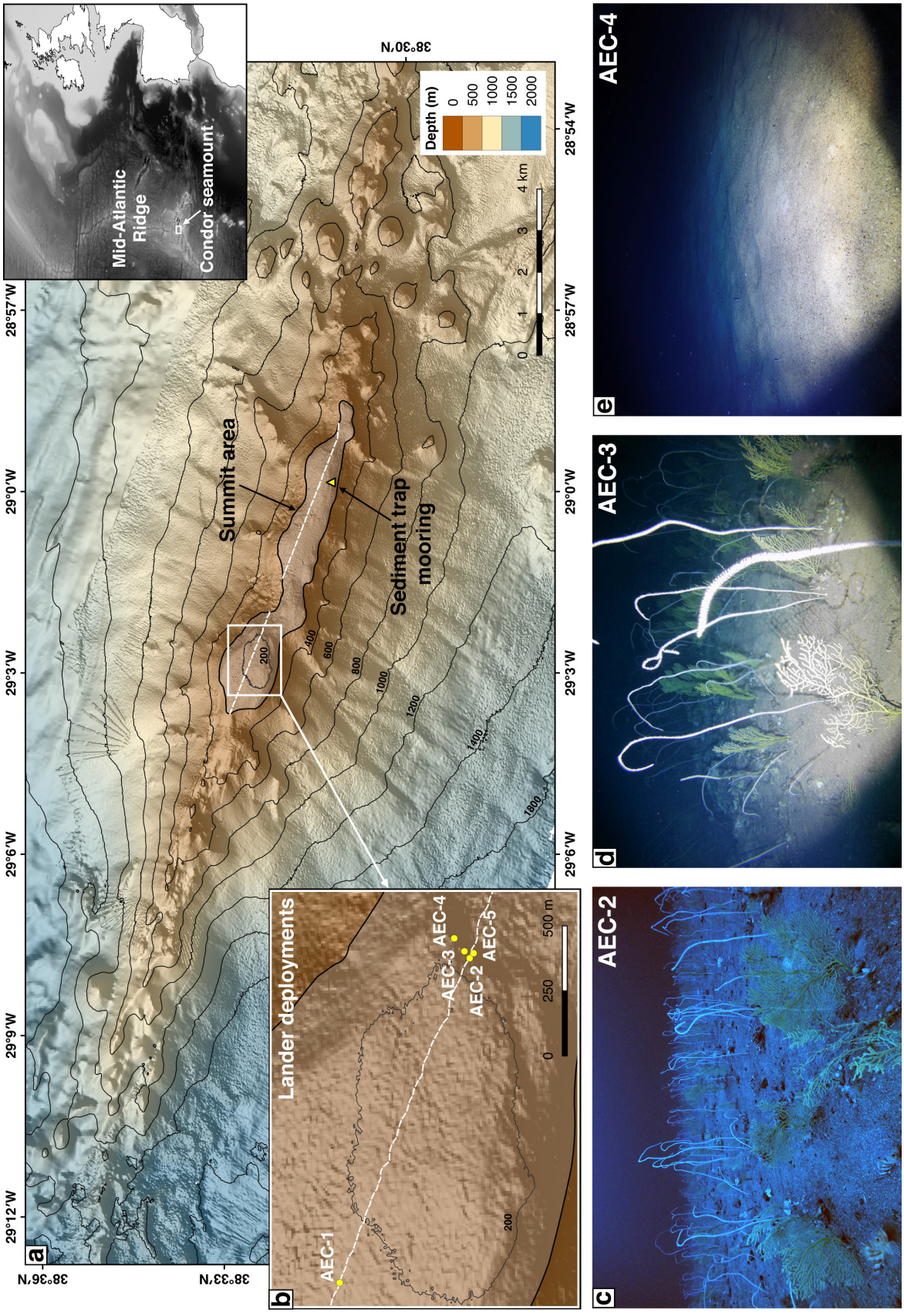

Fig. 1. Case study site. (a) Condor seamount (SW Faial island, Azores) displaying the location of the sediment trap mooring (yellow triangle) and the path of the Hopper towed camera system over the summit (white dashed line), which was used to select suitable areas for aquatic eddy covariance (AEC) deployments. (b) Path of the towed camera system (white dashed line) and location of the 5 AEC deployments on the shallowest part of the summit (coordinates of each deployment provided in Table 2). (c,d) Examples of the images taken with the cameras mounted on the AEC frame showing a dense coral garden formed by the whip octocoral *Viminella flagellum* and the fan-shaped octocoral *Dentomuricea* aff. *meteor*. (e) Image taken from the AEC frame in the sandy area located just a few meters off the coral garden site

lands Institute for Sea Research) during the 2016 MIDAS cruise (cruise code 64PE413). The underwater video device was equipped with a high-definition camera (1920 × 1080 pixels) facing downwards, a pair of parallel lasers 30 cm apart used for image scaling and an ultra-short baseline (USBL) positioning system to acquire accurate geopositioning data from the vehicle when cruising underwater. Only sequences recorded in the summit area of the seamount (<260 m depth) were considered for this study (Dive H04, white dashed lines in Fig. 1a). Two main locations were identified: areas characterized by the presence of dense coral gardens (Fig. 1c,d) and areas with bare sand with no distinguishable epifauna, such as corals and hydrozoans (Fig. 1e). AEC deployments were performed in July and early August of 2018 during short daytrips with the R/V 'Águas Vivas' (Government of the Azores). Three AEC deployments were performed over the selected coral garden (AEC-2, -3, -5), 1 deployment on a sandy patch close to the coral garden (AEC-4, ~100 m offsite) and 1 more deployment (AEC-1) on a large sandy area located 1.4 km away from the coral location (Fig. 1b).

The selected coral garden was located at a depth of approximately 210 m on the western part of the summit (38° 32.381′ N, 29° 02.349′ W; Fig. 1). The patch stretched for approximately 95 m and was dominated by the octocoral species *V. flagellum* and *D.* aff. *meteor*. Densities of both species were estimated using the projection of the parallel lasers over the seafloor, which allowed for a fixed field of view of 2 m to be delimited along the path of the camera system over the coral patch (total area evaluated: 190 m^2). All octocoral colonies observed within the field of view were annotated, and species counts were converted into density estimates by dividing the length of the patch into a string of 10 m^2 sampling units. The average sizes for both coral species were estimated using underwater video images recorded with the remotely operated vehicle mini-ROV SP (SeaBotix LBV300S-6; IMAR-DOP/UAz), equipped with a standard-definition camera (570 lines) and parallel lasers 5 cm apart. The 8 ROV dives used for this study were performed on coral aggregations at the summit of the Condor seamount (175 to 250 m depth) in the years 2010 to 2011 as part of the CoralFISH project. When the reflection of the parallel lasers crossed the base of the corals, video frames were extracted for coral size estimation. The height of 345 *V. flagellum* and 212 *D. meteor* were measured using the software Macnification (Orbicule) from a total of 315 video frames extracted from the video footage.

2.3. Water column characterization

Water column profiles of temperature, salinity, pressure, turbidity (Seapoint Sensor), photosynthetically active radiation (LI-193SA spherical quantum sensor; Li-COR Biosciences) and fluorescence (Cyclops-7; Turner Designs, USA) were collected with a CTD90M multiparameter probe (Sea & Sun Technology). Measurements were conducted during a set of up to 4 casts before and after each AEC deployment. In addition, a 5 l Niskin bottle, mounted 2.5 m above the probe, was used for discrete water sampling. Water samples were analyzed for dissolved nutrients, chl *a* and POM concentrations at a depth of approximately 5 m above the summit (206 to 212 m depth) and within the deep chlorophyll maximum (DCM) at approximately 50 m depth, as indicated by the values of the fluorometer. Each set of CTD casts yielded a total 2 × 5 l of seawater for each targeted depth.

Water samples for nutrient characterization (2 × 20 ml for each set of casts) were filtered onboard using 0.2 µm sterile syringe filters and stored at 0°C under dark conditions for further analyses. The concentration of nitrite (NO_2^-), nitrate (NO_3^-), ammonium (NH_4^+) and orthophosphate (PO_4^{3-}) were determined spectrophotometrically with an automatic continuous segmented flow analyzer (Skalar San^{plus}; Skalar Analytical). For POM determination, 5 l of seawater per set of casts was filtered through a precombusted GF/F filter (0.7 µm; Whatman). The filters were freeze-dried and kept at –20°C pending further analyses. The concentration of particulate nitrogen (PN), particulate organic carbon (POC) and particulate inorganic carbon (PIC) were quantified in duplicate using a Flash Smart CHN elemental analyzer (Thermo Fisher Scientific) on aliquots of known area (ca. 130 mm^2) (see Kiriakoulakis et al. 2004). Determination of chl *a* was performed with a spectrophotometer after filtering 3 l of seawater through 0.7 µm GF/F filters and subsequent extraction into acetone following Holm-Hansen et al. (1965).

2.4. Benthic oxygen uptake

Benthic O_2 uptake was quantified by the non-invasive AEC technique. The AEC system used in this study consisted of a deep-sea rated Acoustic Doppler velocimeter (Vector; Nortek), 1 O_2 microelectrode module (see McGinnis et al. 2011), 1 O_2 optode module (Pyroscience) (see Huettel et al. 2020) and underwater battery canisters mounted on a steel

frame. The parallel O_2 microelectrode and optode modules were deployed concurrently to allow for redundancy and cross-validation. A conductivity-temperature-depth (CTD) probe (SBE19; Seabird) logger equipped with an O_2 optode (Aanderaa) was mounted on the AEC frame to collect auxiliary time series of O_2 to calibrate the readings of the AEC microsensors. The AEC frame was also equipped with 2 Nautilux Custom underwater LED lights and 2 Benthic2 camera housings (Group B Distribution) with GoPro Hero 3 and 4 action cameras (GoPro). The cameras covered 2 of the 3 sides of the AEC frame and were used to visually inspect the benthic habitats and to crosscheck the positioning within the targeted habitats.

Given the rugged nature of the seafloor, the AEC measurement height (h) was fixed to 0.35 m. High-resolution (64 Hz) time series of current velocity and O_2 time series were processed for flux extraction following validated data-processing protocols (see Attard et al. 2014, Rovelli et al. 2015). The time series were averaged and despiked after Goring & Nikora (2002) to reduce the dataset sizes and instrument noise, respectively. The flow velocity coordinate system was rotated using a planar fit algorithm to minimize non-turbulent (advective) flow contributions over complex topographical features (Lorke et al. 2013). Turbulent fluctuations of O_2 and vertical velocity were computed over a time interval of 5 min via linear detrending. For the investigated studies, a stepwise analysis of the window size vs. mean flux (see Attard et al. 2014) indicated that a 5 min window was an optimal trade-off between including the major turbulent contributions while minimizing the inclusion of non-turbulent processes. Linear detrending, alignment of the O_2 and velocity time series (i.e. time shift), as well as the O_2 flux extraction were computed using the Fortran program suite Sulfide-Oxygen-Heat-Flux Eddy Analysis (SOHFEA) version 2.0 (available from www.dfmcginnis.com/SOHFEA; McGinnis et al. 2014). The mean time shift was computed for each time window based on the highest correlation and ranged from −0.8 to −1.2 s, in line with the observed low flow velocities (about 2 to 7 cm s^{-1} on average). In order to better relate the obtained O_2 flux rates to the targeted benthic communities and their heterogeneity, the size of the theoretical AEC footprint area (i.e. the area that contributes to 90% of the flux) and the region of maximum flux contribution (X_{max}) were estimated for each deployment based on h and the bottom roughness length scale (z_0) (Berg et al. 2007). Mean values for z_0 were derived from Reynolds stress assuming Law-of-the-Wall, as described in Inoue et al. (2011). It should be noted that the model of Berg et al. (2007) was applied here outside of the original range of h and z_0, as in other high roughness settings (e.g. Reidenbach et al. 2013, Berg et al. 2019) and might thus be subject to higher uncertainties, as the location of the footprint, and thus the associated integrated flux, shifts with changes in the flow direction (Berg et al. 2007, de Froe et al. 2019, Rodil et al. 2019). While a traditional flux-direction-velocity analysis, based on correlation plots and principal component analysis was also performed at the coral garden sites using OriginPro® (OriginLab), our benthic mapping did not allow for a comprehensive assessment of flow directions, and associated AEC footprint, with footprint-specific biodiversity characterization (e.g. Rodil et al. (2019). Instead, we characterized single habitats within each site using a cumulative flux approach (see de Froe et al. 2019). Here, we parsed together time periods with stable flux contributions, i.e. periods in which the cumulative flux showed a clear linear trend (see Fig. S1 in the Supplement at www.int-res.com/articles/suppl/m688p019_supp.pdf). Depending on flow characteristics (direction and velocity) and benthic faunal densities, the resulting mean flux might include more than 1 directional footprint, typically over a 30 to 90° range and occasionally >90°, and thus provide a better spatial integration of each habitat. Periods characterized by evident deviations from linear trends in the cumulative flux, e.g. spikes and step-like features which would suggest unstable flux conditions, were flagged and not included in subsequent calculations. Mean O_2 uptake rates were reported for the single habitat patches (for the garden sites) as above, based on the obtained fluxes (in 5 min steps) as well as for the whole site (garden and sandy sites), by averaging all stable flux contributions during the entire deployment time. To allow for better comparability with the literature, the uptake rates are presented in mmol m^{-2} d^{-1}. The methodological aspects of AEC applications to CWC habitats have already been evaluated in detail in previous studies (Rovelli et al. 2015, de Froe et al. 2019) and such aspects will only be discussed in general terms in this study.

2.5. Sediment trap

A mooring containing a single cone-shaped sediment trap mounted above an acoustic release was deployed on the summit of the Condor seamount (38° 31.2426′ N, 28° 59.8488′ W; Fig. 1a) on 28 Nov-

ember 2017 at a depth of 218 m. The sediment trap was located approximately 5 m above the bottom. The trap had a surface area of 0.5 m^2 and contained a total of 20 bottles, filled with 2% formaldehyde in a 40 ppt salinity solution. The trap was programmed to collect 20 samples from 1 December 2017 until its retrieval on 7 June 2018 (Table S1). The supernatant in the retrieved bottles was decanted and replaced with a 4% formaldehyde solution and stored for further treatment following Lampitt et al. (2001). Briefly, the samples were filtered, frozen and freeze-dried and the dry mass recorded. POC content was measured on a Thermo Scientific FlashSmart Elemental Analyser (Thermo Fisher Scientific), the samples being de-carbonized prior to analysis (Yamamuro & Kayanne 1995). POC fluxes were calculated by dividing the carbon content of each bottle by the trap area and the number of days the bottle had been open.

3. RESULTS

3.1. Octocoral densities and sizes in the selected coral garden

A total of 438 *Viminella flagellum* and 168 *Dentomuricea* aff. *meteor* colonies (col) were annotated in the targeted 95 m long coral garden. For *V. flagellum*, this corresponded to an average density of 2.30 ± 1.44 col m^{-2} (mean ± SD) and a maximum density inside the patch of 5.7 col m^{-2}. For *D.* aff. *meteor*, the average density was 0.88 ± 0.41 col m^{-2} with a maximum density inside the patch of 1.8 col m^{-2}. The average colony heights determined from the images recorded with the ROV on the seamount summit were 79.8 ± 38.2 cm for *V. flagellum* and 36.2 ± 18.9 cm for *D.* aff. *meteor.*

3.2. Water column

A total of 36 CTD casts were performed during the observational period (6 July to 1 August 2018). Mean temperature ranged from 22.4°C near the surface (4 to 5 m depth) to 15.0°C near the seamount summit (~200 m depth). Salinity changed very little with depth, ranging from 36.2 to 36.0, with most variability in the 0 to 80 m depth range (Fig. 2). Mean photosynthetically active radiation (PAR) declined exponentially from 1200 µmol quanta m^{-2} s^{-1} at the surface to <2 µmol quanta m^{-2} s^{-1} at the seamount summit. Water turbidity was generally low (0.1 to 0.5 nephelometer turbidity units [NTU]), but slightly higher levels were encountered near the surface and at a depth of 35 m. The DCM was located between 46 and 72 m depth and revealed a mean chl *a* concentration of 0.9 µg l^{-1} (Fig. 2, Table 1). Surface and near-bottom chl *a* concentrations amounted to ≤0.1 µg l^{-1}.

Discrete sampling showed low concentrations of NH_4^+ (0.6 to 0.8 µmol l^{-1}) in both the DCM and near the bottom. As expected, NO_3^- concentrations were higher near the bottom (6.0 µmol l^{-1} on average) than within the DCM (1.1 µmol l^{-1}), while NO_2^- was below detection (<0.1 µmol l^{-1}) at both depths (Table 1). Concentrations of PO_4^{3-} ranged from 0.1 to 0.4 µmol l^{-1} between the DCM and near-bottom samples. The concentrations of POC and PN within the DCM were on average 3.6 and 0.5 µmol l^{-1}, respectively. In contrast, the near-bottom concentrations of both POC and PN were 2 times lower, but with comparable POC:PN ratios of 6.1 to 6.2 (Table 1).

Near-bottom velocity within the seamount summit area ranged from 0 to approximately 18 cm s^{-1}, and was on average lower within the coral garden (~2 cm s^{-1}) than for the non-garden sandy sites (4 to 7 cm s^{-1}; Table 2). All

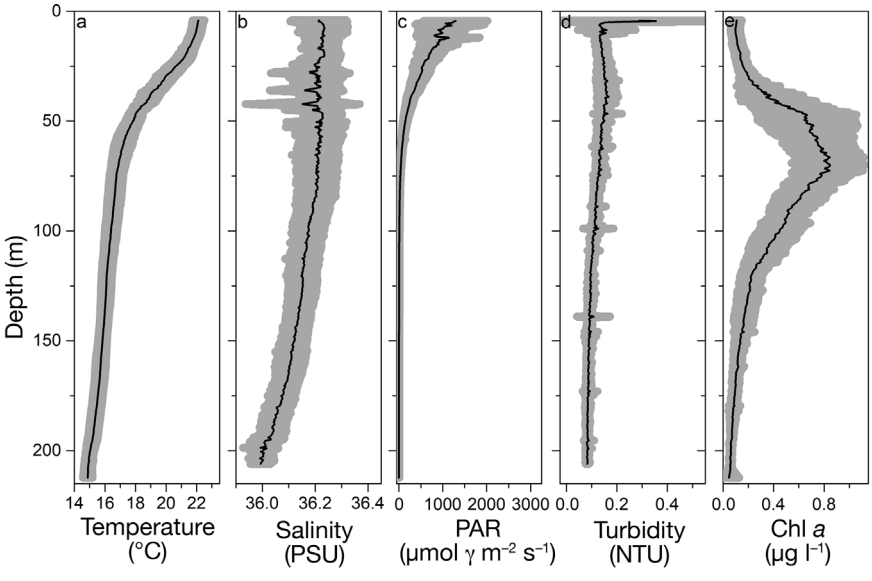

Fig. 2. Mean water column profiles for (a) temperature, (b) salinity, (c) photosynthetically active radiation (PAR), (d) turbidity and (e) chl *a* based on all collected casts (n = 36). The shaded area represents the SD

Table 1. Overview of baseline temperature, chl *a*, nutrients and POM data at the deep chlorophyll maximum (DCM) and near-bottom at the Condor seamount. Mean temperature and concentrations of nitrate (NO_3^-), nitrite (NO_2^-), ammonium (NH_4^+), orthophosphate (PO_4^{3-}), particulate nitrogen (PN), particulate organic carbon (POC) and particulate inorganic carbon (PIC) are presented as mean ± SD; bd: below detection (<0.1 µmol l^{-1})

Parameter	DCM 60 ± 8 m depth	Near-bottom water 203 ± 5 m depth
Temperature (°C)	17.0 ± 0.4	14.9 ± 0.2
Chl *a* (µg l^{-1})	0.84 ± 0.30	0.04 ± 0.02
NO_3^- (µmol l^{-1})[a]	1.1 ± 1.0	6.0 ± 0.9
NO_2^- (µmol l^{-1})	bd	bd
NH_4^+ (µmol l^{-1})	0.6 ± 0.6	bd
PO_4^{3-} (µmol l^{-1})	0.1 ± 0.06	0.4 ± 0.05
PN (µmol l^{-1})	0.45 ± 0.11	0.25 ± 0.08
PC (µmol l^{-1})	3.73 ± 0.62	1.66 ± 0.93
POC (µmol l^{-1})	3.56 ± 0.68	1.55 ± 0.69
PIC (µmol l^{-1})	0.17 ± 0.12	0.14 ± 0.27
POC/PN	6.23 ± 0.67	6.10 ± 1.26

[a]From total NO_3^- and NO_2^- minus NO_2^-

sites showed tidal influence (e.g. Fig. S1) superimposed on the local flow dynamics. Based on the flow characteristics (velocity and direction), it was found that the water mass moved slower within the garden than in off-garden regions, thus increasing the theoretical residence time of any particle transported along with the flow (see particle tracks in Fig. S2).

3.3. Benthic oxygen uptake

The AEC system was successfully deployed 5 times, collecting 126 h of high-resolution flux data (Table 2). At the coral garden sites, hourly averaged benthic O_2 uptake rates typically ranged from 4 to 40 mmol m^{-2} d^{-1} (Fig. S1). Each site was characterized by 5 distinct habitat patches, i.e. periods with stable flux, with mean O_2 uptake rates in the range of 5 to 40 mmol m^{-2} d^{-1} (see Fig. 3). The mean O_2 uptake rate at the respective coral garden sites, comprising all 5 habitats, ranged from 10.0 ± 0.8 to 18.8 ± 2.0 mmol m^{-2} d^{-1} (mean ± SE). Mean values for the derived z_0 of the coral garden sites ranged from 6.4 to 7.3 cm, resulting in a theoretical AEC footprint area of 15 to 22 m^2 with the region of maximum flux (X_{max}) located at a horizontal distance of 0.1 m from the sampling volume (Table S2).

In contrast, hourly averaged benthic O_2 uptake rates at the sandy reference site and the off-garden site ranged from 1 to 12 mmol m^{-2} d^{-1}. The mean O_2

Table 2. Overview of aquatic eddy covariance (AEC) deployments combined with physicochemical parameters, flow velocity magnitude, dissolved O_2 concentration and benthic O_2 uptake rates. Values for the respective parameters are reported as mean ± SD and as a range in brackets. Mean O_2 fluxes are presented as mean ± SE. Duration: number of hours used for O_2 flux calculations; the total duration of the AEC deployment is given in brackets. Depl.: deployment; retr.: retrieval

Site	AEC depl.	Coordinates	Date (depl./retr.)	Depth (m)	Duration (h)	Temperature (°C)	Salinity	Velocity (cm s^{-1})	O_2 (% saturation)	O_2 (µmol l^{-1})	O_2 uptake (mmol m^{-2} d^{-1})
Sand	AEC-1	38° 32.725′ N	11 Jul 2018/	210	19.0	14.5 ± 0.1	36.0 ± 0.02	4.4 ± 2.2	89.2 ± 0.7	221.8 ± 1.3	1.7 ± 0.1
		29° 03.208′ W	12 Jul 2018		[22.0]	[14.3–14.8]	[35.97–36.05]	[0–13.0]	[87.9–91.2]	[219.3–225.2]	
Sand (off-garden)	AEC-4	38° 32.422′ N	21 Jul 2018/	205	19.3	14.9 ± 0.3	36.1 ± 0.04	6.9 ± 3.8	92.7 ± 0.7	228.4 ± 2.0	7.5 ± 0.6
		29° 02.297′ W	23 Jul 2018		[46.2]	[14.5–15.6]	[36.01–36.13]	[0–17.7]	[91.4–94.2]	[223.6–232.0]	
Coral garden	AEC-2	38° 32.381′ N	16 Jul 2018/	203	20	14.7 ± 0.2	36.0 ± 0.03	1.8 ± 1.1	91.9 ± 0.9	227.4 ± 2.4	18.8 ± 2.0
		29° 02.349′ W	17 Jul 2018		[20.9]	[14.4–15.1]	[35.96–36.10]	[0–5.5]	[89.8–94.3]	[223.1–234.3]	
Coral garden	AEC-3	38° 32.395′ N	17 Jul 2018/	206	42.0	14.8 ± 0.2	36.1 ± 0.03	1.9 ± 1.0	91.8 ± 0.8	226.5 ± 1.2	10.0 ± 0.8
		29° 02.331′ W	20 Jul 2018		[68.0]	[14.3–15.2]	[35.98–36.12]	[0–6.1]	[89.5–95.0]	[223.1–235.2]	
Coral garden	AEC-5	38° 32.371′ N	24 Jul 2018/	204	25.3	14.7 ± 0.1	36.0 ± 0.02	2.2 ± 1.1	93.6 ± 0.8	231.7 ± 2.3	11.5 ± 0.5
		29° 02.336′ W	1 Aug 2018		[189.6]	[14.4–15.0]	[36.00–36.08]	[0–6.1]	[92.3–96.1]	[228.1–237.1]	

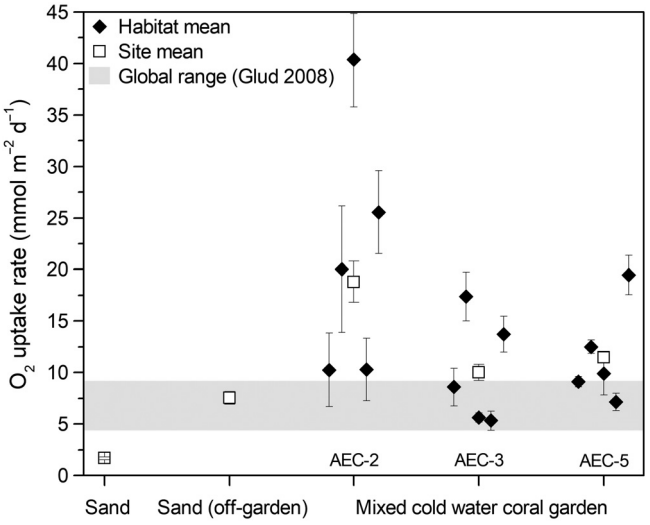

Fig. 3. Overview of all O_2 uptake rates from the mixed octocoral garden and sandy sites (Table 2) from our aquatic eddy covariance deployments. Error bars indicate the SE for habitat patches means and SD for site means. Global range of *in situ* O_2 uptake rates for sedimentary habitats at comparable water depths (175–266 m) is reported after Glud (2008)

uptake at the first sandy reference site was lower, 1.7 ± 0.2 mmol m^{-2} d^{-1} (Table 2, Fig. 3), with hourly averaged rates of up to 4 mmol m^{-2} d^{-1} (Fig. S1). Mean z_0 was reduced to 0.8 cm, resulting in a theoretical AEC footprint area of 102 m^2 (Table S2). At the off-garden sandy site, the O_2 uptake amounted to 7.7 ± 0.8 mmol m^{-2} d^{-1}(Fig. 3), with a mean z_0 of 4.5 cm and an associated theoretical AEC footprint area of 40 m^2 (Table S2).

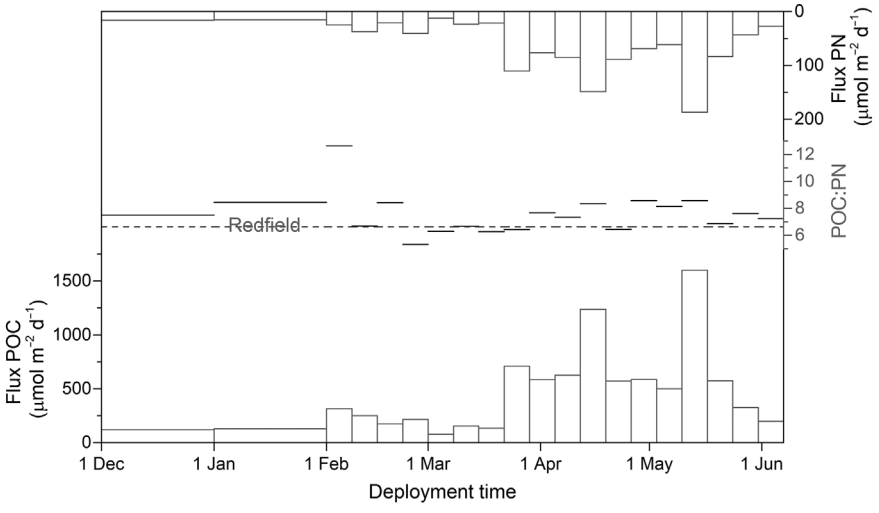

Fig. 4. Fluxes of particulate organic carbon (POC; bottom) and particulate nitrogen (PN; top) from our long-term sediment trap mooring (see Table S1). The POC:PN ratio for each sampling period (center) is provided with the Redfield ratio (6.325) for intercomparisons

At the garden sites, O_2 uptake showed little direct correlation with the magnitude of flow velocity or flow direction, though the last deployment (AEC-5) was characterized by narrower ranges of both velocity and directions (Fig. S3a,b,c). A more detailed analysis of the uptake vs. flow relation using principal component analysis showed that a large portion of the data variance (58.3%) could be attributed to the local hydrodynamics, i.e. flow velocity and direction (Fig. S3d). However, 35.3% of the variance could only be explained in terms of a second component, which is attributable to habitat characteristics, i.e. faunal density and habitat coverage.

3.4. Sediment trap

Deposition rates of POC, as derived from the sediment trap, covered a period of 6 mo (Table S1). Values varied by a factor of approximately 20, from 0.077 mmol C m^{-2} d^{-1} during winter to 1.605 mmol C m^{-2} d^{-1} during late spring, being on average 0.454 ± 0.392 mmol C m^{-2} d^{-1} (mean ± SD). Similarly, PN fluxes were the lowest during winter (<0.020 mmol m^{-2} d^{-1}) and up to 0.186 mmol m^{-2} d^{-1} in late spring. The average during the whole observational period was 0.059 ± 0.047 mmol m^{-2} d^{-1}. The average POC:PN ratio was 7.6 ± 1.5, which is typical for phytodetritus (see Kiriakoulakis et al. 2009). However, we encountered values as high as 12.6 during winter, implying the deposition of more degraded material, and values of only 5.3 during early spring, which are more typical of phytoplankton at the onset of a spring bloom (Fig. 4, Table S1).

4. DISCUSSION

4.1. Cold-water coral habitats as carbon cycling hotspots

This study provides the first *in situ* estimates of O_2 uptake rates for octocoral gardens. Our results show that the community dominated by *Viminella flagellum* and *Dentomuricea* aff. *meteor* at the summit of the Condor seamount represents a hotspot for O_2 uptake. The mean benthic O_2 uptake rate for the coral garden sites (13.5 mmol m^{-2} d^{-1}) was more than a

factor of 2 higher than the mean rate observed at the sandy sites, increasing to a factor of 10 when considering only the sandy summit reference site (Fig. 3, Table 2). The O_2 uptake of 4.6 mmol m^{-2} d^{-1} at the sandy sites is consistent with the global mean benthic *in situ* O_2 uptake rates for other sedimentary habitats at comparable depths (Fig. 3).

The O_2 uptake of the coral gardens falls within the lower end of previously published values for CWC habitats (Table 3). While similar rates have been reported for *in situ* incubations of single branches of the reef-building coral *Lophelia pertusa* (Khripounoff et al. 2014) (Table 3), CWC reef habitats generally appear to have 4 to 10 times higher O_2 consumption rates than the coral gardens at the Condor seamount. This presumably reflects that stony CWC framework-forming scleractinians include a rich associated macrofaunal community living on the underlying dead coral framework (coral rubble), which acts as a biocatalytic filter entrapping POM. Coral rubble has been shown to dominate O_2 uptake in such CWC reef communities (e.g. De Clippele et al. 2021), with average contributions of approximately 23 mmol m^{-2} d^{-1} (Table 3), while the contributions from live coral patches might be as low as 9% of the total O_2 uptake rate (van Oevelen et al. 2009). It should be noted, however, that the activity of suspension feeders displays a strong seasonality (Rossi et al. 2017) and in oligotrophic systems, such as the Azores, octocoral species have been shown to exhibit lower physiological rates in summer months when productivity is low (Coma et al. 2000, Rossi et al. 2006). The current study took place during the summer, which is marked by low surface productivity (Santos et al.

Table 3. Overview of literature oxygen uptake (in mmol m^{-2} d^{-1} ± SE [number of replicates]) by cold-water coral (CWC) communities and from isolated coral specimens. Note that carbon-based uptake rates were converted to O_2 assuming a 1:1 ratio (see Glud 2008). Methods include aquatic eddy covariance (AEC), open water budget (OW), incubations *in situ* (ICis), incubations *ex situ* (ICes) and model-based upscaling (M). na: not available

Site *Location*	Depth (m)	O_2 uptake rate (mmol m^{-2} d^{-1}) [n]	O_2 uptake rate Global[a]	Method	Description	Reference
Condor seamount *Azores, Portugal*	204	13.4 [3][b]	5.5	AEC	Coral garden	This study
Haas mound *Rockall Bank, NE Atlantic*	536	17.0 [2][c]	2.7	AEC	Coral rubble community	de Froe et al. (2019)
Oreo mound *Rockall Bank, NE Atlantic*	745	45.3 ± 11.7 [1]	2.1	AEC	Coral rubble & live *Lophelia* patches	de Froe et al. (2019)
Mingulay Reef Complex *Hebrides Sea, off Scotland*	128	27.8 ± 2.3 [1]	7.8	AEC	Coral rubble community	Rovelli et al. (2015)
Stjernsund *Northern Norway*	220	24.8 ± 2.6 [1]	5.2	AEC	Coral rubble community	Rovelli et al. (2015)
Træna Marine Protected Area *Continental shelf of Norway*	294	121.5 ± 9.9[d] [2]	4.2	AEC	Live CWC reef	Cathalot et al. (2015)
Træna Marine Protected Area *Continental shelf of Norway*	280	81.7 ± 9.8 [1]	4.2	ICis	Estimated via upscaling	Cathalot et al. (2015)
Tisler Reef *Northern Skagerak, Norway*	122	40.0 [8]	8.1	OW	Live *Lophelia pertusa* on coral framework	White et al. (2012)
Guilvinec & Croisic canyon *Brittany, NE Atlantic*	850–880	7.7 [na]	1.9	ICis	Branch of *L. pertusa* or *Madrepora oculata* (3 branches m^{-2})	Khripounoff et al. (2014)
Condor seamount *Azores, Portugal*	200–270	0.07	3.1–5.6	ICes	*Viminella flagellum*	Rakka et al. (2021)
	200–270	0.02	3.1–5.6	ICes	*Dentomuricea* aff. *meteor*	Rakka et al. (2021)
Cap de Creus *Catalunya, Spain*	35–70	0.005 ± 0.005	12.2–20.4	OW	*Paramuricea clavata* gardens	Coppari et al. (2019)
Rockall Bank *NE Atlantic*	294	54.4 ± 4.7[d] [2]	2.0	AEC	Sponge ground	Cathalot et al. (2015)

[a]Global mean O_2 uptake for sedimentary habitats at comparable water depths, after Glud (2008)
[b]Mean from 3 sites (10.0 ± 0.8, 11.5 ± 0.5, 18.8 ± 2.0 mmol m^{-2} d^{-1}, respectively, Table 2)
[c]Mean from 2 habitats (22.4 ± 5.6 and 11.5 ± 3.6 mmol m^{-2} d^{-1}, respectively)
[d]Mean ± SD

2013) and low POC fluxes (sediment trap data presented herein) and therefore the reported O_2 uptake rates of these communities are likely conservative as annual estimates.

These coral gardens primarily develop on consolidated substrates (i.e. fragmented rocks partially covered by depositional sand), with octocoral colonies only covering a small fraction of the available surface (see Fig. 1). Our experimental approach did not allow us to assess the contribution of octocorals themselves to the habitat-integrated O_2 uptake rate. However, an approximate estimate was obtained from parallel laboratory-based feeding experiments on the same species collected from the Condor seamount (Rakka et al. 2021; Table 3). Those experiments determined O_2 respiration rates of 6.24 ± 4.56 µmol g^{-1} d^{-1} (dry weight) for *V. flagellum* and 31.92 ± 7.68 µmol g^{-1} d^{-1} for *D.* aff. *meteor*, respectively. If we extrapolate the dry weight O_2 uptake rates obtained in aquaria to areal rates considering maximum coral densities and average coral sizes measured at the Condor summit (where AEC measurements were taken) and convert them to coral biomass, then the contribution from *V. flagellum* and *D.* aff. *meteor* would be 0.45 and 0.06 mmol m^{-2} d^{-1}, respectively (~5% of the mean O_2 uptake). This suggests that approximately 95% of the observed O_2 uptake rate within the coral garden might be attributed to sedimentary respiration and garden-inhabiting fauna rather than corals themselves.

Our measurement setup did not allow for a direct comparison of O_2 uptake rates and specific characteristics of the integrated footprint areas (i.e. substrate coverage and faunal density), whose contributions to community O_2 uptake is expected to be well integrated by the AEC technique (see Rovelli et al. 2015, de Froe et al. 2019). As discussed above, octocoral densities alone cannot account for the enhanced O_2 uptake rates observed across the sites, where the mean habitat O_2 uptake rates varied by up to 8-fold between the lowest and highest values (Fig. 3). Such variation could in part be attributed to differences in proportions of coverage by depositional sand and colonized hard substrate (see Fig. 1, Text S1) compared to dampened sand deposition and the more colonized hard substrate, as in AEC-2 (see Fig. 1). At the site level, however, community-integrated mean O_2 uptake rates appear to be driven by a complex interplay between habitat characteristics, directly linked to the integrated O_2 uptake, and the local hydrodynamics, which jointly explained most of the data variance (94%; Fig. S3).

4.2. Supply of organic matter to the coral garden

The enhanced carbon cycling of the coral garden implies locally elevated organic matter (OM) supply either through physical processes (i.e. sedimentation and advection) or via an efficient entrapment of OM by the coral communities (e.g. Kiriakoulakis et al. 2004). The hydrodynamic regime at the Condor seamount is characterized by a strong anticyclonic Taylor cap, which prevails throughout most of the year, combined with strong tidal mixing and downwelling events over the summit (Bashmachnikov et al. 2013). Although Taylor caps can enhance local productivity by enriching surface waters with nutrients, in the case of the Condor seamount, the effect appears to be limited to depths below 170 m, and therefore primary production above the summit is low (Bashmachnikov et al. 2013, Ciancia et al. 2016). However, the anticyclonic circulation causes the retention of organic carbon over the summit, which may provide occasional food pulses that can be utilized and recycled within the coral garden. This is consistent with our particle track analyses (Fig. S2), which showed substantially shortened tracks (i.e. longer residence times) at coral garden sites compared to the sandy sites, indicating that the coral garden is exposed for a longer period of time to any OM transports to the seamount summit when compared to the sandy areas. The supply of POM to the summit of the Condor seamount can be estimated from the sediment trap mooring data. If we assume that all sedimentary POM is respired based on standard Redfield stoichiometry (N:C:O = 16:106:138; Redfield et al. 1963), then the combined respiration of POC and PN would account for most of the O_2 uptake at the sandy reference sites, but only below 10% (1.1 mmol m^{-2} d^{-1}) of the mean O_2 uptake for the coral gardens. It should be noted, however, that sediment traps can underestimate vertical fluxes, especially in regions with complex topography and hydrodynamics, as advective pathways are often undersampled (e.g. Jahnke et al. 1990). Furthermore, short time series measurements (weeks to months) of POC fluxes often miss episodic inputs (Smith et al. 1992). Indirect estimates of the POC supply to the summit from export and subsequent deposition of surface net primary production (NPP), inferred from remote sensing (see http://sites.science.oregonstate.edu/ocean.productivity; Behrenfeld & Falkowski 1997) and established export/burial parametrizations (Suess 1980, Dunne et al. 2007) also suggest that while local NPP, albeit low, would be sufficient to sustain coral garden habitats during part of the year

(e.g. in spring), additional supply pathways would likely be required to do so throughout the year, and especially during summer time (see Fig. S4).

Past studies on the OM composition of sediments at the Condor seamount showed impoverished OM content of the sediments on the summit compared to its flanks and an off-seamount station (Bongiorni et al. 2013). This was reflected in a lower abundance and biomass of meiofauna in the summit sediments compared to other stations (Zeppilli et al. 2013). Such observations were interpreted to result from the hydrographic conditions on the seamount, where its main currents presumably transport high concentrations of nutrients, plankton and OM, hitting the Condor seamount from the north and then shifting southward, away from the seamount summit and the southern flank (Bashmachnikov et al. 2013, Bongiorni et al. 2013). Thus, it is possible that the considerable amount of available POM that is delivered at depth to the summit area is consumed, or its entrapment facilitated by suspension feeders with little deposition in seafloor sediments.

During the study period, chl *a* concentrations were low (Fig. 2), in agreement with previous summer surveys (e.g. Santos et al. 2013) and satellite data (Ciancia et al. 2016), with the lowest values near the bottom (Table 1). Comparable trends were also observed for POM concentrations (Table 1). The low chl *a* concentration in near-bottom POM could indicate a small contribution of (viable) phytoplankton. The reported mean POC:PN ratio (6.1 ± 1.26) was close to Redfield stoichiometry (6.6), implying that the POM was not significantly degraded. This is in line with the presence of frequent downwelling events over the summit of the Condor seamount (Tempera et al. 2012, Bashmachnikov et al. 2013), which may occasionally supply fresh phytoplankton and POM to the coral garden from surface waters. Thus, the O_2 uptake rates observed at the coral garden suggest that these communities efficiently entrap material that sustains high biological activity.

The results of this study serve to further validate the strength of the AEC approach to quantify O_2 uptake from CWC habitats, but also highlight the importance that coral gardens may have for local carbon cycling. Given the ubiquitous occurrence of coral gardens, their importance in regional and global biogeochemical cycles should be recognized, especially as changes in the global climate are projected to modify the quantity and quality of the food delivered to deep-sea communities (Sweetman et al. 2017, Puerta et al. 2020). The Azores region is projected to experience critical changes in aragonite saturation and POC flux (Puerta et al. 2020), with concomitant predicted reductions of suitable habitats for octocorals (Morato et al. 2020). The baseline information presented here on carbon turnover of coral gardens is essential to understand future changes in the functioning of these important ecosystems.

Acknowledgements. This project has received funding from the European Union's Horizon 2020 research and innovation programme under grant agreement no. 678760 (ATLAS) and grant agreement no. 689518 (MERCES). Underwater video images were obtained with funding from the European Community 7th Framework Programme under grant agreement no. 213144 (CoralFISH) and grant agreement no. 603418 (MIDAS), and the Corazon Project (FCT/PTDC/MAR/72169/2006) financed by the Fundação para a Ciência e a Tecnologia (FCT). This work was supported by the Danish National Research Foundation through the Danish Center for Hadal Research, HADAL (No. DNRF145) awarded to R.N.G. This output reflects only the authors' view and the European Union cannot be held responsible for any use that may be made of the information contained therein. M.C.S., C.D.-C., M.R. and T.M. also acknowledge funds and support from the FCT through the strategic project (UIDB/05634/2020 and UIDP/05634/2020) granted to OKEANOS and through the FCT Regional Government of the Azores under the project M1.1.A/REEQ.CIENTÍFICO UI&D/2021/010. This study contributes to the project HADES-ERC funded by the European Research Council Advanced Investigator Grant 669947 and to the FNU-7014-00078 grant, awarded by the Danish Council for Independent Research, both awarded to R.N.G. K.M.A. was supported through a Postdoctoral fellowship from the Walter and Andrée de Nottbeck Foundation. L.R. received funding from the German Science Foundation (grant RO 5921/1-1). C.D.-C. was supported by the PO2020 project DeepWalls (ACORES-01-0145-FEDER-000124) and by the FCT-IP Project UIDP/05634/2020. M.R. was funded by a DRCT PhD grand grant (reference M3.1.a/F/047/2015.). M.C.S. and T.M. were supported by Program Stimulus of Scientific Employment (CCCIND/03346/2020 and CCCIND/03345/2020, respectively) from the Fundação para a Ciência e Tecnologia. We thank António Godinho and the crew of the R/V 'Águas Vivas' for their substantial support during the field activities and the scientific team involved in the collection of underwater video images. We are also thankful to Anni Glud and Rikke Orloff Holm for their support in the nutrients analyses.

LITERATURE CITED

Attard KM, Glud RN, McGinnis DF, Rysgaard S (2014) Seasonal rates of benthic primary production in a Greenland fjord measured by aquatic eddy correlation. Limnol Oceanogr 59:1555–1569

Bashmachnikov I, Loureiro CM, Martins A (2013) Topographically induced circulation patterns and mixing over Condor seamount. Deep Sea Res II 98:38–51

Behrenfeld MJ, Falkowski PG (1997) Photosynthetic rates derived from satellite-based chlorophyll concentration. Limnol Oceanogr 42:1–20

Berg P, Røy H, Wiberg PL (2007) Eddy correlation flux meas-

urements: The sediment surface area that contributes to the flux. Limnol Oceanogr 52:1672–1684
Berg P, Delgard ML, Polsenaere P, McGlathery KJ, Doney SC, Berger AC (2019) Dynamics of benthic metabolism, O_2, and pCO_2 in a temperate seagrass meadow. Limnol Oceanogr 64:2586–2604
Bongiorni L, Ravara A, Parretti P, Santos RS, Rodrigues CF, Amaro T, Cunha MR (2013) Organic matter composition and macrofaunal diversity in sediments of the Condor Seamount (Azores, NE Atlantic). Deep Sea Res II 98: 75–86
Buhl-Mortensen L, Buhl-Mortensen P (2018) Cold temperate coral habitats. In: Beltran CD, Camacho ET (eds) Corals in a changing world. InTech, London, p 9–28
Buhl-Mortensen L, Vanreusel A, Gooday AJ, Levin LA and others (2010) Biological structures as a source of habitat heterogeneity and biodiversity on the deep ocean margins. Mar Ecol 31:21–50
Buhl-Mortensen L, Serigstad B, Buhl-Mortensen P, Olsen MN, Ostrowski M, Błażewicz-Paszkowycz M, Appoh E (2017) First observations of the structure and megafaunal community of a large *Lophelia* reef on the Ghanaian shelf (the Gulf of Guinea). Deep Sea Res II 137: 148–156
Carmo V, Santos M, Menezes GM, Loureiro CM, Lambardi P, Martins A (2013) Variability of zooplankton communities at Condor seamount and surrounding areas, Azores (NE Atlantic). Deep Sea Res II 98:63–74
Carreiro-Silva M, Ocaña O, Stanković D, Sampaio Í, Porteiro FM, Fabri MC, Stefanni S (2017) Zoantharians (Hexacorallia: Zoantharia) associated with cold-water corals in the Azores Region: new species and associations in the deep sea. Front Mar Sci 4:88
Cathalot C, Van Oevelen D, Cox TJS, Kutti T, Lavaleye M, Duineveld G, Meysman FJR (2015) Cold-water coral reefs and adjacent sponge grounds: hotspots of benthic respiration and organic carbon cycling in the deep sea. Front Mar Sci 2:37
Ciancia E, Magalhães Loureiro C, Mendonça A, Coviello I and others (2016) On the potential of an RST-based analysis of the MODIS-derived chl-a product over Condor seamount and surrounding areas (Azores, NE Atlantic). Ocean Dyn 66:1165–1180
Coma R, Ribes M, Gili JM, Zabala M (2000) Seasonality in coastal benthic ecosystems. Trends Ecol Evol 15:448–453
Coppari M, Zanella C, Rossi S (2019) The importance of coastal gorgonians in the blue carbon budget. Sci Rep 9: 13550
Davies AJ, Guinotte JM (2011) Global habitat suitability for framework-forming cold-water corals. PLOS ONE 6: e18483
De Clippele LH, Rovelli L, Ramiro-Sánchez B, Kazanidis G and others (2021) Mapping cold-water coral biomass: an approach to derive ecosystem functions. Coral Reefs 40: 215–231
de Froe E, Rovelli L, Glud RN, Maier SR and others (2019) Benthic oxygen and nitrogen exchange on a cold-water coral reef in the North-East Atlantic Ocean. Front Mar Sci 6:665
Dodds LA, Roberts JM, Taylor AC, Marubini F (2007) Metabolic tolerance of the cold-water coral *Lophelia pertusa* (Scleractinia) to temperature and dissolved oxygen change. J Exp Mar Biol Ecol 349:205–214
Dunne JP, Sarmiento JL, Gnanadesikan A (2007) A synthesis of global particle export from the surface ocean and cycling through the ocean interior and on the seafloor. Global Biogeochem Cycles 21:GB4006
Glud RN (2008) Oxygen dynamics of marine sediments. Mar Biol Res 4:243–289
Gomes-Pereira JN, Carmo V, Catarino D, Jakobsen J and others (2017) Cold-water corals and large hydrozoans provide essential fish habitat for *Lappanella fasciata* and *Benthocometes robustus*. Deep Sea Res II 145: 33–48
Goring DG, Nikora VI (2002) Despiking acoustic Doppler velocimeter data. J Hydraul Eng 128:117–126
Henry LA, Roberts JM (2017) Global biodiversity in cold-water coral reef ecosystems. In: Rossi S, Bramanti L, Gori A, Orejas C (eds) Marine animal forests. Springer International Publishing, Cham, p 235–256
Holm-Hansen O, Lorenzen CJ, Holmes RW, Strickland JDH (1965) Fluorometric determination of chlorophyll. ICES J Mar Sci 30:3–15
Huettel M, Berg P, Merikhi A (2020) Technical note: Measurements and data analysis of sediment–water oxygen flux using a new dual-optode eddy covariance instrument. Biogeosciences 17:4459–4476
Inoue T, Glud RN, Stahl H, Hume A (2011) Comparison of three different methods for assessing in situ friction velocity: a case study from Loch Etive, Scotland. Limnol Oceanogr 9:275–287
Jahnke RA, Reimers C, Craven DB (1990) Intensification of recycling of organic matter at the sea floor near ocean margins. Nature 348:50–54
Khripounoff A, Caprais J, Le Bruchec J, Rodier P, Noel P, Cathalot C (2014) Deep cold-water coral ecosystems in the Brittany submarine canyons (Northeast Atlantic): hydrodynamics, particle supply, respiration, and carbon cycling. Limnol Oceanogr 59:87–98
Kiriakoulakis K, Bett BJ, White M, Wolff GA (2004) Organic biogeochemistry of the Darwin Mounds, a deep-water coral ecosystem, of the NE Atlantic. Deep Sea Res I 51: 1937–1954
Kiriakoulakis K, Vilas JC, Blackbird SJ, Arístegui J, Wolff GA (2009) Seamounts and organic matter — is there an effect? The case of Sedlo and Seine seamounts, Part 2. Composition of suspended particulate organic matter. Deep Sea Res II 56:2631–2645
Lampitt R, Bett B, Kiriakoulakis K, Popova E, Ragueneau O, Vangriesheim A, Wolff G (2001) Material supply to the abyssal seafloor in the Northeast Atlantic. Prog Oceanogr 50:27–63
Long MH, Berg P, de Beer D, Zieman JC (2013) In situ coral reef oxygen metabolism: an eddy correlation study. PLOS ONE 8:e58581
Lorke A, McGinnis DF, Maeck A (2013) Eddy-correlation measurements of benthic fluxes under complex flow conditions: effects of coordinate transformations and averaging time scales. Limnol Oceanogr 11:425–437
McGinnis DF, Cherednichenko S, Sommer S, Berg P and others (2011) Simple, robust eddy correlation amplifier for aquatic dissolved oxygen and hydrogen sulfide flux measurements. Limnol Oceanogr 9:340–347
McGinnis DF, Sommer S, Lorke A, Glud RN, Linke P (2014) Quantifying tidally driven benthic oxygen exchange across permeable sediments: an aquatic eddy correlation study. J Geophys Res Oceans 119:6918–6932
Morato T, González-Irusta J, Dominguez-Carrió C, Wei C and others (2020) Climate-induced changes in the suitable habitat of cold-water corals and commercially

important deep-sea fishes in the North Atlantic. Glob Change Biol 26:2181–2202

Pham CK, Gomes-Pereira JN, Isidro EJ, Santos RS, Morato T (2013) Abundance of litter on Condor seamount (Azores, Portugal, Northeast Atlantic). Deep Sea Res II 98:204–208

Porteiro FM, Gomes-Pereira JN, Pham CK, Tempera F, Santos RS (2013) Distribution and habitat association of benthic fish on the Condor seamount (NE Atlantic, Azores) from *in situ* observations. Deep Sea Res II 98:114–128

Puerta P, Johnson C, Carreiro-Silva M, Henry LA and others (2020) Influence of water masses on the biodiversity and biogeography of deep-sea benthic ecosystems in the North Atlantic. Front Mar Sci 7:239

Rakka M, Maier SR, Van Oevelen D, Godinho A, Bilan M, Orejas C, Carreiro-Silva M (2021) Contrasting metabolic strategies of two co-occurring deep-sea octocorals. Sci Rep 11:10633

Redfield AC, Ketchum BH, Richards FA (1963) The influence of organisms on the composition of the sea water. In: Hill MN (ed) The sea, Vol 2. Interscience Publisher, New York, NY, p 26–77

Reidenbach MA, Berg P, Hume A, Hansen JCR, Whitman ER (2013) Hydrodynamics of intertidal oyster reefs: the influence of boundary layer flow processes on sediment and oxygen exchange. Limnol Oceanogr Fluids Environ 3:225–239

Roberts JM, Wheeler AJ, Freiwald A (2006) Reefs of the deep: the biology and geology of cold-water coral ecosystems. Science 312:543–547

Roberts JM, Davies AJ, Henry LA, Dodds LA and others (2009) Mingulay reef complex: an interdisciplinary study of cold-water coral habitat, hydrography and biodiversity. Mar Ecol Prog Ser 397:139–151

Rodil IF, Attard KM, Norkko J, Glud RN, Norkko A (2019) Towards a sampling design for characterizing habitat-specific benthic biodiversity related to oxygen flux dynamics using Aquatic Eddy Covariance. PLOS ONE 14:e0211673

Rossi S, Gili JM, Coma R, Linares C, Gori A, Vert N (2006) Temporal variation in protein, carbohydrate, and lipid concentrations in *Paramuricea clavata* (Anthozoa, Octocorallia): evidence for summer–autumn feeding constraints. Mar Biol 149:643–651

Rossi S, Bramanti L, Gori A, Orejas C (eds) (2017) Marine animal forests. The ecology of benthic biodiversity hotspots. Springer International Publishing, Cham

Rovelli L, Attard KM, Bryant LD, Flögel S and others (2015) Benthic O_2 uptake of two cold-water coral communities estimated with the non-invasive eddy correlation technique. Mar Ecol Prog Ser 525:97–104

Rovelli L, Attard KM, Cárdenas CA, Glud RN (2019) Benthic primary production and respiration of shallow rocky habitats: a case study from South Bay (Doumer Island, Western Antarctic Peninsula). Polar Biol 42:1459–1474

Santos M, Moita MT, Bashmachnikov I, Menezes GM and others (2013) Phytoplankton variability and oceanographic conditions at Condor seamount, Azores (NE Atlantic). Deep Sea Res II 98:52–62

Smith KL, Baldwin RJ, Williams PM (1992) Reconciling particulate organic carbon flux and sediment community oxygen consumption in the deep North Pacific. Nature 359:313–316

Suess E (1980) Particulate organic carbon flux in the oceans — surface productivity and oxygen utilization. Nature 288:260–263

Sweetman AK, Thurber AR, Smith CR, Levin LA and others (2017) Major impacts of climate change on deep-sea benthic ecosystems. Elem Sci Anth 5:4

Tempera F, Giacomello E, Mitchell NC, Campos AS and others (2012) Mapping Condor seamount seafloor environment and associated biological assemblages (Azores, NE Atlantic). In: Harris PT, Baker EK (eds) Seafloor geomorphology as benthic habitat. Elsevier, p 807–818

Tempera F, Hipólito A, Madeira J, Vieira S, Campos AS, Mitchell NC (2013) Condor seamount (Azores, NE Atlantic): a morpho-tectonic interpretation. Deep Sea Res Part II 98:7–23

van Oevelen D, Duineveld G, Lavaleye M, Mienis F, Soetaert K, Heip CHR (2009) The cold-water coral community as a hot spot for carbon cycling on continental margins: a food-web analysis from Rockall Bank (northeast Atlantic). Limnol Oceanogr 54:1829–1844

White M, Bashmachnikov I, Arstegui J, Martins A (2008) Physical processes and seamount productivity. In: Pitcher TJ, Morato T, Hart PJB, Clark MR, Haggan N, Santos RS (eds) Seamounts: ecology, fisheries & conservation. Blackwell Publishing Ltd, Oxford, p 62–84

White M, Wolff G, Lundälv T, Guihen D, Kiriakoulakis K, Lavaleye M, Duineveld G (2012) Cold-water coral ecosystem (Tisler Reef, Norwegian Shelf) may be a hotspot for carbon cycling. Mar Ecol Prog Ser 465:11–23

Yamamuro M, Kayanne H (1995) Rapid direct determination of organic carbon and nitrogen in carbonate-bearing sediments with a Yanaco MT-5 CHN analyzer. Limnol Oceanogr 40:1001–1005

Yesson C, Taylor ML, Tittensor DP, Davies AJ and others (2012) Global habitat suitability of cold-water octocorals. J Biogeogr 39:1278–1292

Zeppilli D, Bongiorni L, Cattaneo A, Danovaro R, Santos RS (2013) Meiofauna assemblages of the Condor Seamount (North-East Atlantic Ocean) and adjacent deep-sea sediments. Deep Sea Res II 98:87–100

Editorial responsibility: Chris Langdon, Coral Gables, Florida, USA
Reviewed by: C. E. Reimers and 2 anonymous referees

Submitted: July 26, 2021
Accepted: February 21, 2022
Proofs received from author(s): April 22, 2022